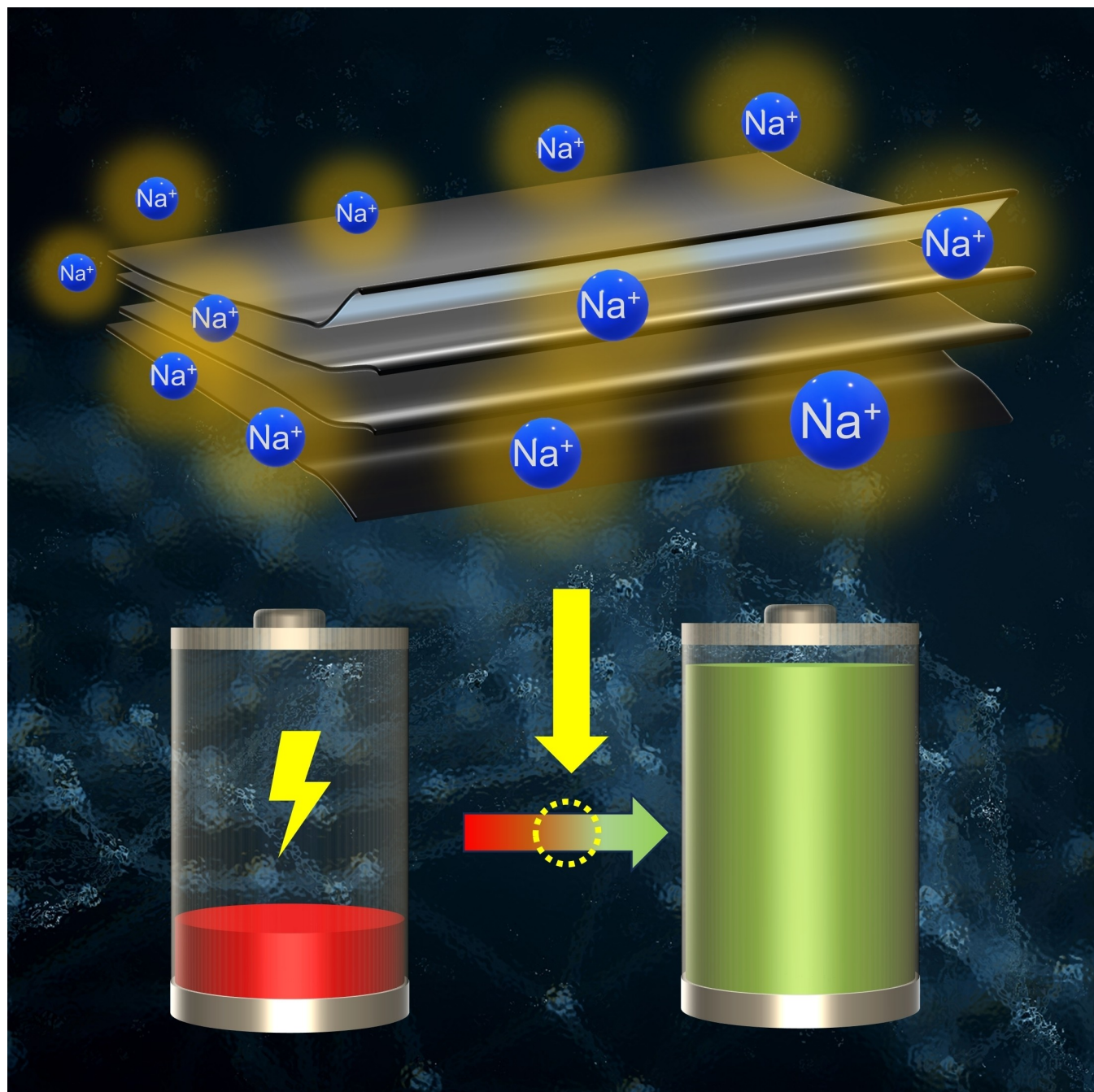


# Graphite Co-Intercalation Chemistry in Sodium-Ion Batteries

Linlong Lyu,<sup>[a]</sup> Yuyang Yi,<sup>[a]</sup> and Zheng-Long Xu<sup>\*[a, b]</sup>



Lithium ion intercalation chemistry in graphite underpins commercial lithium-ion batteries since 1991. In exploring the potential of cost-effective graphite anodes in alternative battery systems, the conventional intercalation chemistry falls short for Na ions, which exhibited minimal capacity and thermodynamic unfavourability in sodium ion batteries (SIBs). The introduction of an alternative intercalation chemistry involving solvated-Na-ion co-intercalation gives a rebirth to graphite anodes. The co-intercalation chemistry allows appreciable Na ion storage capacities and extraordinary rate capabilities. The fundamental

differences between intercalation and co-intercalation chemistries have attracted extensive investigation over the past decade for high-power SIBs. Herein, we focus on the state-of-the-art advances on the co-intercalation chemistry in the SIBs for the purpose of enriching insights into graphite intercalation chemistry. Following our introducing the thermodynamic features of co-intercalation reactions, we will illuminate the electrochemical properties and mechanic issues of co-intercalated graphite, finalized by the perspective challenges and potential resolutions.

## 1. Introduction

The ever-growing electrical vehicle market boosts the demanding of lithium-ion batteries (LIBs) due to their high power and energy densities and flexible design.<sup>[1]</sup> The uneven distribution and surging price of raw materials like Li and Co have raised widespread argument on the large-scale affordability of LIBs,<sup>[2]</sup> thus calling for alternative batteries using more abundant elements. Among them, sodium ion batteries (SIBs) have been considered as a promising substitute due to the high chemical similarity between Na with Li, the high abundance and low cost of Na.<sup>[3]</sup> A shortcut toward the implementation of SIBs would be directly "grafting" the know-how developed in commercial LIBs. To minimize complexity of the "grafting", the widely affordable graphite would be preferred to pair with various cathodes. Natural graphite shows an interlayer spacing of 3.35 Å among graphene layers, which enable guest intercalation to form graphite intercalation compounds (GICs).<sup>[4,5]</sup> Full intercalation of  $\text{Li}^+$  (radius = 0.76 Å) could generate a binary GIC (b-GIC,  $\text{LiC}_6$ ) with a theoretical capacity of 372 mAh g<sup>-1</sup> at a low working potential of ~0.15 V vs. Li/Li<sup>+</sup>.<sup>[6]</sup> The interlayer space of graphite was assumed sufficient to accommodate  $\text{Na}^+$  (radius = 1.02 Å).<sup>[7]</sup> Therefore, graphite was considered an ideal anode material choice in SIBs.

Unfortunately, the amount of Na, that can reversibly intercalate into the graphite at room temperature, is limited to a stoichiometry of  $\text{NaC}_{184}$ .<sup>[8]</sup> At an elevated temperature of 80 °C, graphite still exhibited a marginal capacity of 35 mAh g<sup>-1</sup> ( $\text{NaC}_{64}$ ).<sup>[9]</sup> The inferior capacity is omnipresent in ester-based or polymer electrolytes with  $\text{NaPF}_6$ <sup>[8]</sup> or  $\text{NaCF}_3\text{SO}_3$  salt.<sup>[9]</sup> Calculations suggested the thermodynamic instability of Na-b-GICs, either  $\text{NaC}_{16}$  or  $\text{NaC}_{12}$ .<sup>[10]</sup> The enthusiasm of adopting graphite

anode for SIBs thus diminished. Until 2014, Jache et al introduced solvated-Na-ion intercalation chemistry (denoted as the co-intercalation chemistry) to form ternary GICs (t-GICs), which realized highly reversible sodiation/desodiation for the first time.<sup>[11]</sup> Kim et al unveiled the detailed structural evolutions of graphite during sodiation/desodiation by using in-situ X-ray diffraction (XRD) characterizations and theoretical calculations.<sup>[12]</sup> The Na-ion co-intercalation reaction was then intensively studied for SIBs. The new intercalation chemistry of graphite has also been extended to other battery systems like Mg ion batteries<sup>[13,14]</sup> and Ca ion batteries.<sup>[15-19]</sup>

The preparation of t-GICs has a long history, but it takes a time to establish feasibilities in SIBs (Figure 1).<sup>[20]</sup> Graphite is a highly anisotropic layered host consisting of van der Waals force stacked graphene layers, and the graphene layer is built by strong covalently bonded carbon hexagons through  $\text{sp}^2$  hybridization. Graphite galleries enable the intercalation of many guests, including metal cations,<sup>[21,22]</sup> anions,<sup>[23,24]</sup> molecules,<sup>[21,22]</sup> cation-solvents,<sup>[25,26]</sup> and anion-solvents.<sup>[27,28]</sup> Various GICs endows their versatile applications in superconductors,<sup>[29,30]</sup> batteries,<sup>[31]</sup> and electrocatalyst.<sup>[20,32]</sup> In rechargeable batteries, b-GICs have long been more favorable than t-GICs because of the higher capacity and better cyclic stability of b-GICs. A representative example is the  $\text{Li}^+$  intercalated graphite ( $\text{LiC}_6$ , b-GIC), which is superior to  $\text{Li}^+$ -PC intercalated graphite (t-GIC) in LIBs.<sup>[33,34]</sup> Nevertheless, only t-GICs can enable high-capacity graphite anodes in SIBs and boost the (de)intercalation kinetics for high-rate cycling (*i.e.*, 10 Ag<sup>-1</sup>).<sup>[35]</sup> The extraordinary kinetic can be ascribed to the circumvention of the desolvation step, which always requires extra energy to separate cations from coordinated solvent molecules.<sup>[11,12,35]</sup>

The reborn of commercial graphite in the SIBs offers an unprecedented opportunity toward high-power Li-free rechargeable batteries. Na-ion co-intercalation chemistry can also be extended to non-graphite anodes, like hydrotitanates<sup>[36]</sup> and  $\text{TiS}_2$ <sup>[37,38]</sup> for long-cycling SIBs.<sup>[39-41]</sup> Although several appealing review papers summarized the merits and potential commercialization of co-intercalating graphite SIB,<sup>[42,43]</sup> co-intercalation chemistry is far from being completely understood in comparison to the conventional intercalation chemistry. Therefore, it is imperative to summarize the state-of-the-art insights into co-intercalation chemistry with emphases on the electrochemical merits and the underlying mechanism. We will start by analyzing the thermodynamic aspects of Na ion intercalation in

[a] Dr. L. Lyu, Dr. Y. Yi, Prof. Z.-L. Xu  
 Research Institute for Advanced Manufacturing, Department of Industrial Systems and Engineering, The Hong Kong Polytechnic University, Hung Hom, Kowloon, Hong Kong SAR, China  
 E-mail: zhenglong.xu@polyu.edu.hk

[b] Prof. Z.-L. Xu  
 Research Centre for Nature-Inspired Science and Engineering (RCNISE), The Hong Kong Polytechnic University, Hung Hom, Kowloon, Hong Kong SAR, China

© 2024 The Authors. *Batteries & Supercaps* published by Wiley-VCH GmbH. This is an open access article under the terms of the Creative Commons Attribution Non-Commercial License, which permits use, distribution and reproduction in any medium, provided the original work is properly cited and is not used for commercial purposes.

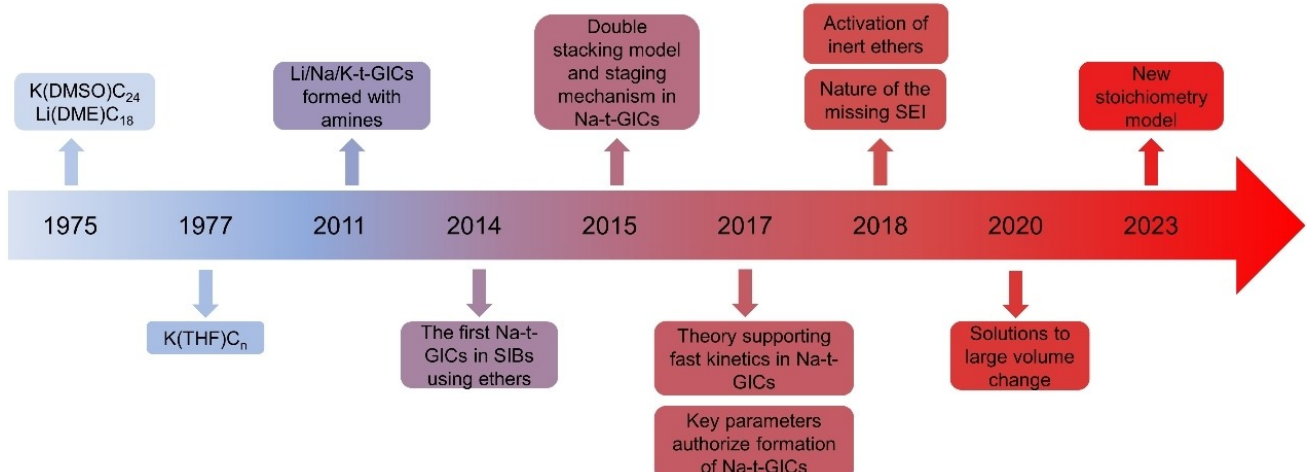


Figure 1. Timeline of key advances in t-GICs in the SIBs, adopted from Refs. [25,26,44,45,55,59,67,69–71,76].

graphite, and the feasibility of Na ion co-intercalation chemistry for graphite anodes. Then, we will highlight the ultrafast intercalation kinetics and the high design flexibility of co-intercalation reactions. The large volume changes and controversial solid electrolyte interphase (SEI) issues will also be illustrated for graphite anodes. At the end, we will identify the formidable challenges and propose potential resolutions toward the practical application of graphite anodes in SIBs.

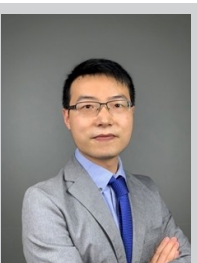
## 2. Unfavourability of Bare $\text{Na}^+$ Intercalation in Graphite

Thermodynamically, Na enjoys lower first ionization energy and electronegativity than Li, which may facilitate its chemical bonding to graphite.<sup>[7]</sup> However, the graphite anode exhibits

negligible Na intercalation capacities ( $< 10 \text{ mAh g}^{-1}$ ) at room temperature in ester-based electrolytes (Figure 2a). When the electrolytes contain linear ether solvents, graphite exhibited significant capacities of  $\sim 100 \text{ mAh g}^{-1}$  through a co-intercalation reaction (Figure 2b). The voltage profiles display a flat plateau at  $\sim 0.6 \text{ V}$  vs.  $\text{Na}/\text{Na}^+$  and two slope regions in  $1.0\text{--}0.63$  and  $0.59\text{--}0.01 \text{ V}$  vs.  $\text{Na}/\text{Na}^+$ .<sup>[11]</sup> The result is distinct from those for  $\text{Li}^+$  and  $\text{K}^+$  intercalation in graphite, which display discharge plateaus at  $\sim 0.1 \text{ V}$  vs.  $\text{Li}/\text{Li}^+$  with a capacity of  $\sim 360 \text{ mAh g}^{-1}$  ( $\text{LiC}_6$ ) and  $\sim 0.2 \text{ V}$  vs.  $\text{K}/\text{K}^+$  with a capacity of  $\sim 240 \text{ mAh g}^{-1}$  ( $\text{KC}_8$ ). The difference can be explained by the thermodynamic disparities between  $\text{LiC}_6$ ,  $\text{KC}_8$  b-GICs and  $(\text{Na}-\text{DME})_x$  t-GICs. The formation of b-GICs requires energies to extract cations from solvate species, whereas only partial desolvation happens in co-intercalation reaction,<sup>[12,44,45]</sup> thus leading to the higher redox plateaus.



Linlong Lyu is currently a postdoctoral fellow in the Department of Industrial and Systems Engineering at The Hong Kong Polytechnic University. He received his B.Sc in Materials Science and Engineering from Sichuan University, M.Sc, and Ph.D. degree from The Hong Kong Polytechnic University. He focuses on mechanistic investigation of post-Li batteries and the design of new electrode materials and energy storage devices.



Zheng-Long Xu is currently an assistant professor in the Department of Industrial and Systems Engineering at The Hong Kong Polytechnic University. He received his B.Sc in Materials Science and Engineering from Zhejiang University and Ph.D. degree from The Hong Kong University of Science and Technology. His research group at PolyU focuses on the development of new materials and devices for post-Li battery chemistries (i.e., Li-S, Na-ion, and Ca-ion batteries) and operando characterizations (i.e., in situ TEM).



Yuyang Yi received her Ph.D. in New Energy Science and Engineering from Soochow University, Suzhou, China, in 2022. She is currently working as a postdoctoral fellow in the Department of Industrial and Systems Engineering at the School of the Hong Kong Polytechnic University. Her research interests include the design of new energy storage materials and the electrochemical reaction mechanisms.

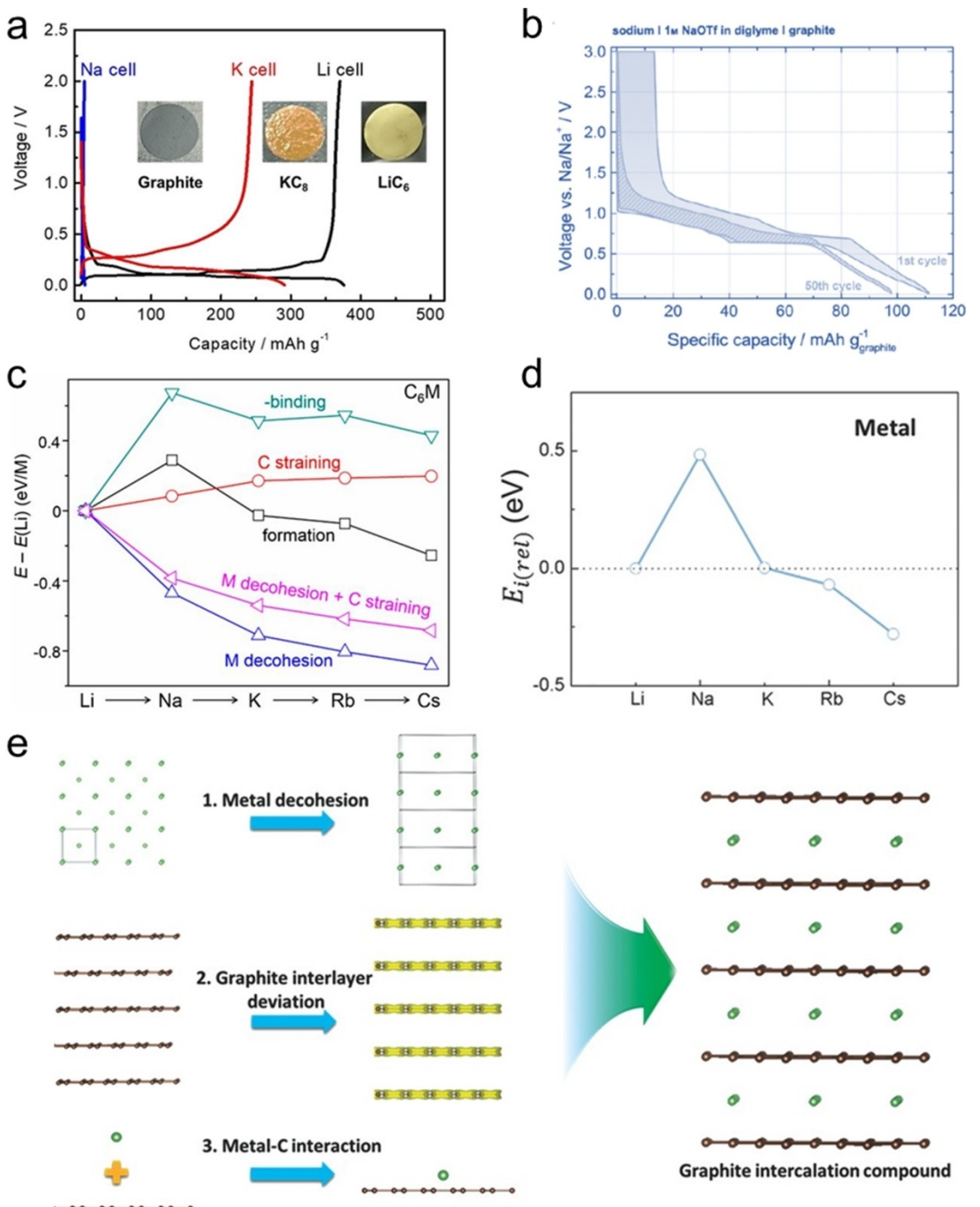


**Figure 2.** (a) Typical voltage profiles of graphite in ester-based lithium, sodium, and potassium electrolytes. Reproduced from ref. [83] with permission from John Wiley and Sons. (b) Voltage profiles of graphite in diglyme-based sodium electrolyte. Reproduced from ref. [11] with permission from John Wiley and Sons. (c) The energetics of each step, relative to those of Li. Reproduced from ref. [13] with permission from United States National Academy of Sciences. (d) Energy factors from interaction between alkali metal and single graphene layer. (e) Factors contributing to  $E_f$  values of b-GICs. (d) and (e) are reproduced from ref. [44] with permission from John Wiley and Sons.

The early explanation to the low-capacity of graphite anode in ester electrolyte is the larger ionic radius of Na<sup>+</sup> (1.02 Å) than Li<sup>+</sup> (0.76 Å), which prohibited the accommodation of Na<sup>+</sup> in graphite galleries. Expanding the interlayer space of carbon materials was thus proposed to enlarge Na<sup>+</sup> storage capacities. For example, Stevens et al expanded the interlayer space and

created numerous interior nanopores in hard carbons to enlarge the sodiation capacity to ~300 mAh g<sup>-1</sup>.<sup>[46]</sup> The hollow carbon nanowires were also synthesized with interlayer spaces of above 3.7 Å for high Na ion storage capacities ~250 mAh g<sup>-1</sup> over 400 cycles.<sup>[47]</sup> The expanded graphite oxides with an interlayer space of 4.3 Å displayed a sodiation capacity of

284 mAh g<sup>-1</sup>, which also supported the size effect between Na<sup>+</sup> and the interlayer space of graphite.<sup>[48]</sup> Despite these progress, all above reports used carbon anodes with disordered structure or abundant functional groups, which can significantly cover the capacity contribution from Na ion intercalation reaction. Graphite can store larger ions like K<sup>+</sup> (1.38 Å) and PF<sub>6</sub><sup>-</sup> than Na<sup>+</sup>. It means the low capacity of graphite anodes may not be caused by the size mismatch between Na<sup>+</sup> and graphite galleries.

By density functional theory (DFT) calculations, Okamoto et al demonstrated a negative intercalation potential for the stage I Na-b-GICs, either NaC<sub>8</sub> or NaC<sub>6</sub>. It means that Na metal can plat prior to the formation of NaC<sub>8</sub> or NaC<sub>6</sub> compounds.<sup>[49]</sup> To consolidate this theoretical study, a spherical graphite anode was discharged using chronopotentiograms and potentiostatic intermittent titration techniques, which displayed large enough Na ion diffusion inside spherical graphite. The result demonstrated that the limitation of Na<sup>+</sup> intercalation into graphite might be originated from the thermodynamic limitation instead of the kinetic limitation inside graphite.<sup>[50]</sup> The thermodynamic unfavourability of Na-b-GICs formation was also investigated by DFT calculations. It was primarily reported that the formation of NaC<sub>16</sub> and NaC<sub>12</sub> suffers highly stressed graphite structure in plane C-C bonds upon Na<sup>+</sup> intercalation.<sup>[10]</sup> According to Hess's law, the formation of Na-b-GICs was then deconvoluted into three steps, namely, (i) the reconstruction of graphite to Na intercalated graphite structure; (ii) the reconstruction of bcc Na metal to Na in graphite; (iii) the intercalation of Na into graphite. Reaction (i) and (ii) are endothermic but reaction (iii) is exothermic.<sup>[51]</sup> The total exothermic enthalpy was calculated to be insufficient for the formation of NaC<sub>6</sub>. The reaction (iii) can be further specified as the charge transfer from Na<sup>+</sup> to graphene layer and the formation of Na-C chemical bonds. The binding energy changes can be deconvoluted into the energy change from Na ionization ( $E_{ion}$ ), and the coupling of Na<sup>+</sup> and graphene (electrostatic and other quantum-mechanical interactions,  $E_{cp}$ ). By calculating these parameters among alkali metals, it was found that Na exhibited the weakest binding to graphene ( $E_{cp}$ ). The  $E_{ion}$  decreases from Li<sup>+</sup>, Na<sup>+</sup> to K<sup>+</sup> in the periodic table, thus the  $E_{cp}$  should increase with their correspondingly increasing distance from graphene layers. An abrupt ionization drop was observed for Na, which was ascribed to the competition between  $E_{ion}$  and  $E_{cp}$  for the abnormal formation energy of NaC<sub>6</sub> (Figure 2c).<sup>[13]</sup> The interactions between intercalated Na<sup>+</sup> and graphene remains unreasonable if we only consider the general  $E_{cp}$ . Yoon et al elucidated that the large repulsive local interaction between Na<sup>+</sup> and graphene layer is the main reason for destabilization of low stage Na-b-GICs (Figure 2d).<sup>[44]</sup> The theoretical model exhibiting formation of low stage Na-b-GICs is illustrated in Figure 2e. Therefore, the strong intercalations between Na<sup>+</sup> and graphite cause the infeasibility of Na-b-GICs and the limited capacities of graphite anodes.

### 3. Intercalation of Solvated Na<sup>+</sup> into Graphite

#### 3.1. Structural Evolution of Graphite Undergoing Co-Intercalation Reaction

As aforementioned, the graphite anode in SIBs was unlocked by altering the solvent from esters to linear ethers through a co-intercalation reaction. The intercalation of solvent molecules in Na-t-GICs can be claimed by ex-situ Fourier-transform infrared spectroscopy (FTIR) characterizations of discharged electrodes.<sup>[35]</sup> The phase evolution of graphite anode can be revealed by *in-situ* XRD measurement using 1 M NaPF<sub>6</sub> diglyme electrolyte.<sup>[12]</sup> Figure 3a shows the reversible staging behavior of graphite during discharging and charging. During sodiation, the (002) peak splits into two new peaks. Prior to the formation of stage III GICs, the graphite experiences a one-phase like reaction. Conversion of stage III to stage II GICs is achieved through a biphasic reaction, concomitant fading of stage III and evolving of stage II. Transition from stage II to stage I GICs is similar. At the end of sodiation, the diffraction pattern of single-phase stage I GICs was well-maintained except appearance of new peaks at 12–14° referring to in-plane super-structural ordering of Na<sup>+</sup> and diglyme. The fully sodiated GIC presented a significantly enlarged lattice parameter of ~11.6 Å, corresponding to a  $\Delta V = \sim 246\%$ , which is much larger than the ~10.6% for Li-b-GICs and ~59.7% for K-b-GICs.<sup>[52]</sup> The formation of Na-t-GICs was also demonstrated by the *in-situ* Raman measurement (Figure 3b).<sup>[53]</sup> The typical staging behaviors of GICs to the final stage I phase were illustrated by gradual weakening of G<sub>UC</sub> peak (G peak of uncharged graphene layer) and the steadily enhancing G<sub>C</sub> peak (G peak of charged graphene layer in contact with intercalate layer). Raman peaks were identified by the different Fermi levels of ~0.8 eV for stage II Na-t-GICs and ~1.2 eV for stage I Na-t-GICs.

The stoichiometry of stage I Na-t-GICs has also been confirmed via rigorous experimental and theoretical studies. Na-t-GICs was denoted as [Na(solvent)<sub>x</sub>]C<sub>y</sub>, where x refers to the coordination number of solvent molecules per Na ion and y corresponds to the number of carbon atoms per Na ion. According to the experimental results in literature, x can be 1 or 2 and y is in the range of 16 and 26.<sup>[11,12,45,54–56]</sup> y values are mainly calculated from the electrochemically measured maximum capacities. Different testing conditions like electrolyte components, electrode thickness, graphite structure, can lead to fluctuations of the maximum capacities and the consequent y values. The value of x can be experimentally determined by measuring the mass change of t-GICs as a function of (de)sodiation capacities, which exhibits a linear slope corresponding to the x value. x=2 was also supported by the DFT calculated solvation structure of Na ions in dilute electrolyte solution<sup>[11,57,58]</sup> and the elemental analysis of chemically prepared Na-t-GICs.<sup>[56]</sup> Interestingly, x=1 has also been underpinned by the fitting results of measured electrode mass change upon sodiation, the O: Na ratio = 3:1 by EDS mapping, and first-principles calculations.<sup>[12,44,45]</sup> Clearly, no consensus has been reached on the stoichiometry of stage I Na-t-GICs.

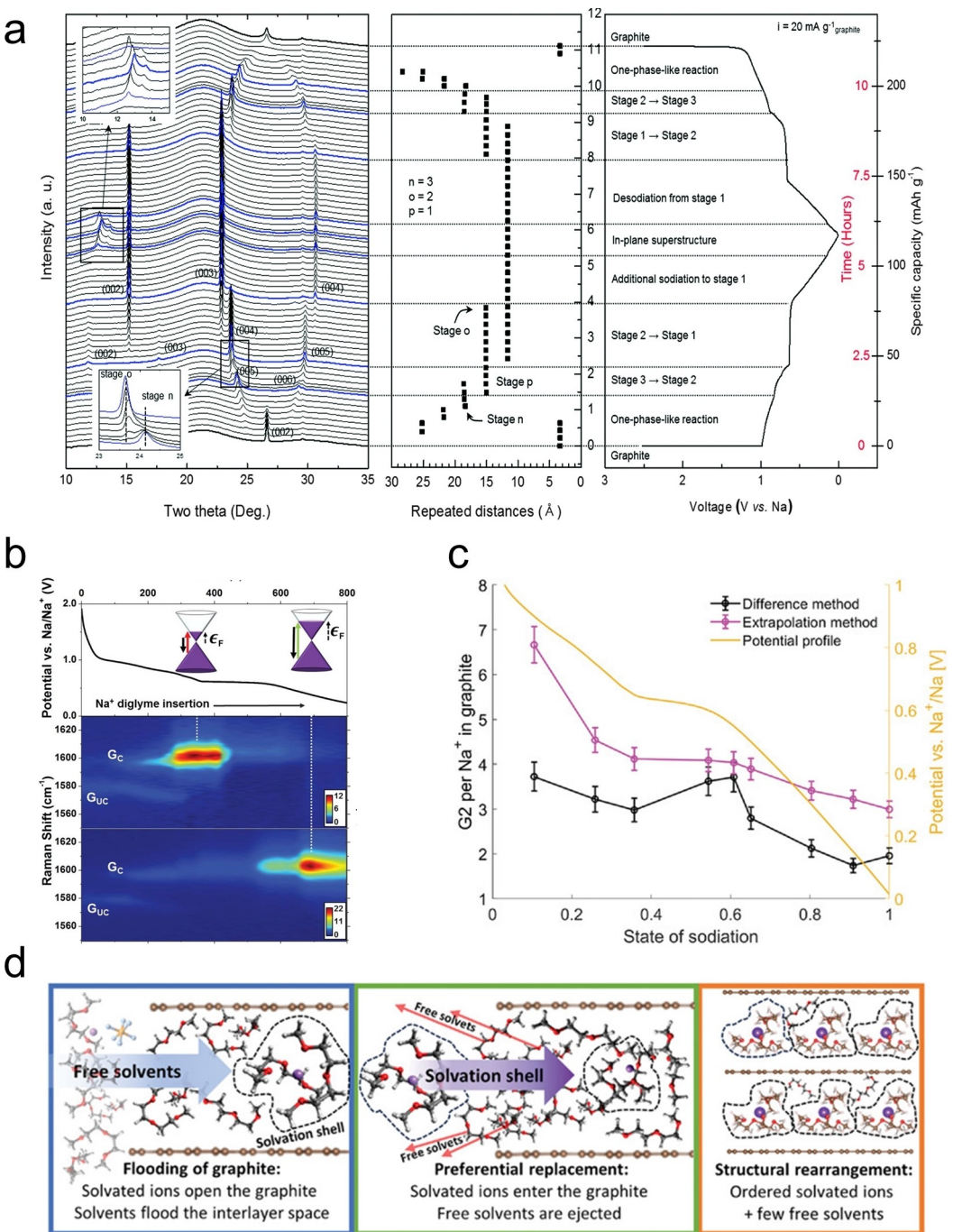


**Figure 3.** (a) Operando synchrotron XRD analysis of the structural evolution of graphite anode. Reproduced from ref. [12] with permission from Royal Society of Chemistry. (b) In-situ Raman spectra of Na-t-GICs obtained using 1.58 eV laser (top) and 2.33 eV laser (bottom). Reproduced from ref. [53] with permission from American Chemical Society. (c) The calculated ratio of diglyme (G<sub>2</sub>) to Na<sup>+</sup> in graphite using mass difference and extrapolation method. (d) Schematic of proposed new model of diglyme solvated Na<sup>+</sup> intercalation in graphite. (c) and (d) are reproduced from ref. [59] with permission from John Wiley and Sons.

Recently, Åvall et al. revisited the weight-change measurement method and excluded the high temperature drying process, thus to exclude any loss of intercalant and the solvating diglyme molecules. Figure 3c shows that the  $x$  value is changing with the sodiation process instead of a fixed value of 1 or 2.<sup>[59]</sup> A new model in Figure 3d explained that after the initial intercalation of Na<sup>+</sup>-diglyme complexes into graphite galleries, the expanded layered structure allows free solvents

flooding inside. With further sodiation, the intercalating solvated-Na<sup>+</sup> can replace the pre-intercalated free solvent molecules, thus decreasing the diglyme: Na<sup>+</sup> ratio (or  $x$  value). The ratio was maintained at the plateau region (~0.6 V) and decreased steadily to the end of sodiation. The final stoichiometry of Na-t-GICs was determined as [Na(diglyme)<sub>x</sub>]C<sub>20</sub> ( $x=2$ ) with considerable amount of free solvent molecules inside. This

work provides a dynamic picture to the stoichiometry of Na-t-GICs during co-intercalation reaction in SIBs.

### 3.2. Fast Kinetics of Co-Intercalation Reaction

The most outstanding gain of the co-intercalation reaction is the high-power capability for potentially fast charging SIB applications. As shown in Figure 4a, at a high current density of  $5 \text{ A g}^{-1}$ , reversible capacity of  $\sim 100 \text{ mAh g}^{-1}$  is deliverable for natural graphite.<sup>[35]</sup> It was also reported that at an ultra-high current density of  $30 \text{ A g}^{-1}$ , the reversible capacity of  $\sim 100 \text{ mAh g}^{-1}$  and well-defined voltage plateaus were still retained for few-layered graphene, which are inaccessible for the conventional Li-ion intercalation reaction.<sup>[53]</sup> The intercalation kinetics of electrodes are usually affected by electronic and ionic conductivities and the mass transfer speed. It was argued that the electronic conductivities of graphite would be benefited from alkaline metal ion intercalation, regarding the metallic nature of b-GICs.<sup>[60,61]</sup> For the Na-t-GICs, there is partial electron transfer from Na to graphene layers. The s electron of Na would dwell at anti-bonding  $\pi^*$  orbital of graphene layer.<sup>[62]</sup> The electron concentration can be accumulated up to  $\sim 2.5 \times 10^{14} \text{ cm}^{-2}$  per graphene layer with increase in the state of charge. These findings imply the enhanced electronic conductivity of graphite anodes after co-intercalation reactions.

With respect to ionic conductivity and mass transfer kinetics, the electrochemical behaviors of graphite anodes can provide intriguing insights. By CV scanning at different sweeping rates, the storage of solvated-Na-ion in graphite was divided into

diffusion-limited and capacitive-controlled regions (Figure 4b). The capacitive-controlled process generally exhibits fast charge transfer, while the diffusion-limited region can also display rapid kinetics. One factor that can promote the intercalation kinetics is the marginal solid electrolyte interface (SEI) layer formed from electrolyte decomposition in ether-based electrolytes.<sup>[35,55]</sup> Thick SEI layers usually demand full desolvation of ions in bulky electrolyte, thus slowing down the following intercalation kinetics, which is a well-known rate limiting step in the LIBs.<sup>[63,64]</sup> Figure 4c shows that no obvious reduction in both charge transfer resistance and interfacial resistance to cross SEI for the co-intercalation reaction. Jung et al calculated the diffusion coefficient of solvated  $\text{Na}^+$  in graphite galleries to be  $1.1 \times 10^{-8} \text{ cm s}^{-1}$ , which is originated from low diffusion barrier (0.13 eV) of  $\text{Na}^+$ -diglyme. The van der Waals interaction between diglyme and graphene constructs a flat energy surface to facilitate rapid sliding of solvated diglyme parallel to graphene surface (Figure 4d).<sup>[45]</sup> Raman results also suggested weakened interactions between ion and graphene, thus facilitating the trivial in-plane deformation and the improved in-plane diffusion kinetics.<sup>[53]</sup> The Na-ion diffusion kinetics in graphite was also measured by in-situ electrochemical scanning tunnelling microscopy (Figure 4e).<sup>[65]</sup> By quantifying local graphite lattice change and tracking its propagation over the electrode, the Na-ion diffusion rates are  $\sim 5.9 \times 10^{-7} \text{ cm s}^{-1}$  and  $\sim 2.2 \times 10^{-6} \text{ cm s}^{-1}$  for 1 M  $\text{NaClO}_4$  in triglyme and tetraglyme, respectively. Overall, the fast kinetics of  $\text{Na}^+$ -ether intercalation chemistry make graphite a competitive anode in the SIBs.

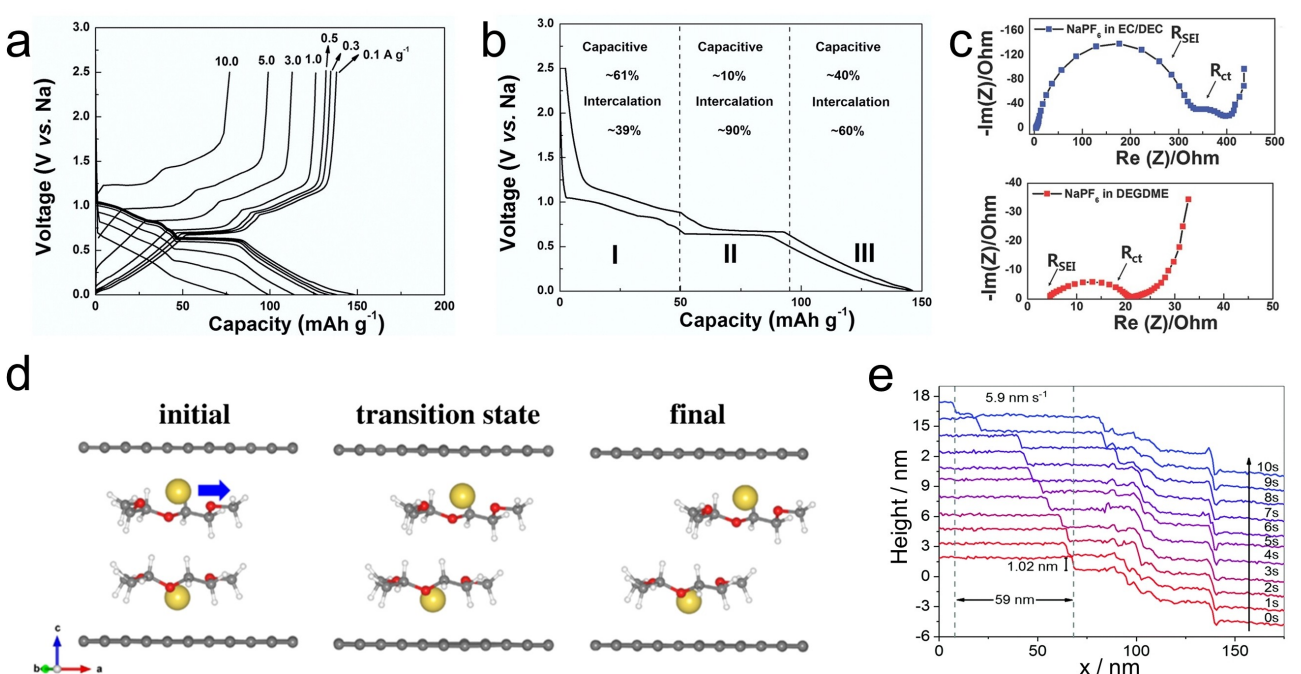


**Figure 4.** (a) Rate capability of graphite in a typical diglyme-based electrolyte. (b) Quantified capacitive and intercalative contribution in typical voltage profile of Na-t-GICs. (c) Nyquist plots of graphite in ester-based electrolyte (top) and ether-based electrolyte (bottom). (a-c) are reproduced from ref. [35] with permission from John Wiley and Sons. (d) Vital states of  $\text{Na}^+$ -diglyme diffusions in graphite and corresponding structure. Reproduced from ref. [45] with permission from Elsevier. (e) Temporal propagation of the graphite lattice expansion measured in 1 M  $\text{NaClO}_4$  in triglyme at room temperature. Reproduced from ref. [65] with permission from Elsevier.

### 3.3. Solvent-Dependent Co-Intercalation Behaviors

There are various solvents that can coordinate  $\text{Na}^+$  to intercalate into graphite by forming Na-t-GICs. The prevailing solvents are linear ethers, including monoglyme, diglyme, and tetraglyme.<sup>[12,35,54,66]</sup> Less attention has been paid to ethers like triethylene glycol dimethyl ether (triglyme), pentaethylene glycol (pentaglyme),<sup>[67]</sup> or poly(ethylene glycol) dimethyl ether, which require high operation temperatures or large overpotentials to activate the co-intercalation reactions. The solvent species have shown impact on the redox potentials of Na ion intercalation in graphite. For example, a steady shift of major redox peaks to lower voltages when chain length of linear ether shortens. Specifically, there is a 0.18 V reduction in working potential when the monoglyme replaces tetraglyme, as displayed in Figure 5a.<sup>[12]</sup> Xu et al further elucidated the redox potentials' dependency on the chain length of ether solvents and interpreted the dependency via the standard formation potential of t-GICs and activity of free solvent ( $a_{\text{fs}}$ ).<sup>[66]</sup> According to following equation:

$$V = (E_{\text{t-GICs}}^{\circ} - E_{\text{Na}}^{\circ}) + \frac{2.303RT}{nF} \log a_{\text{fs}} \quad (1)$$

where  $V$ ,  $E_{\text{t-GICs}}^{\circ}$ ,  $E_{\text{Na}}^{\circ}$ ,  $R$ ,  $T$ ,  $n$ , and  $F$  are the intercalation voltage, standard electrode potential of t-GICs and sodium metal, gas constant, temperature, amount of charge transfer, and Faraday

constant, respectively. Variation of the solvent activity in electrolytes and the standard potential of final product corresponding  $a_{\text{fs}}$  and  $E_{\text{t-GICs}}^{\circ}$  would affect the reaction voltage. Specifically, the increase in chain length of linear ether could enlarge the interlayer distance of graphene sheets, which diminished the effective repulsion among graphene layers with  $\text{Na}$  ions, thus enhancing the stability of t-GICs and increasing the  $E_{\text{t-GICs}}^{\circ}$  (or higher  $V$ ). The high working potential of graphite anode is detrimental to the high energy density of Na-ion full cells.

To decrease the redox potential of graphite, an effective approach is to decrease  $a_{\text{fs}}$  as shown in Equation (1). Increment of salt concentrations could coordinate solvent molecules, thus reducing the number of free solvents in electrolyte. The increased intensity ratios of coordinating solvents to free solvents, referring to the reduction of  $a_{\text{fs}}$ , was revealed by Raman spectra. According to Equation (1), the decline of  $a_{\text{fs}}$  leads to the reduction of redox potentials. It is worth noting that the variation of intensity ratio is nonlinear. The ratio increased from 0.04 (0.05 M) to 0.23 (1.5 M) and 15.7 (3.0 M), indicating a significant decrease of free solvents in high concentrations. In the highly concentrated electrolyte (3 M),  $a_{\text{fs}}$  gave an extremely low value and reduced co-intercalation voltage by ~0.2 V. Improving the temperature is another method in promoting monotonous reduction in redox potentials. Specifically, elevation of temperature promotes the entropy of t-GICs and increases the ratio of solvent solvation

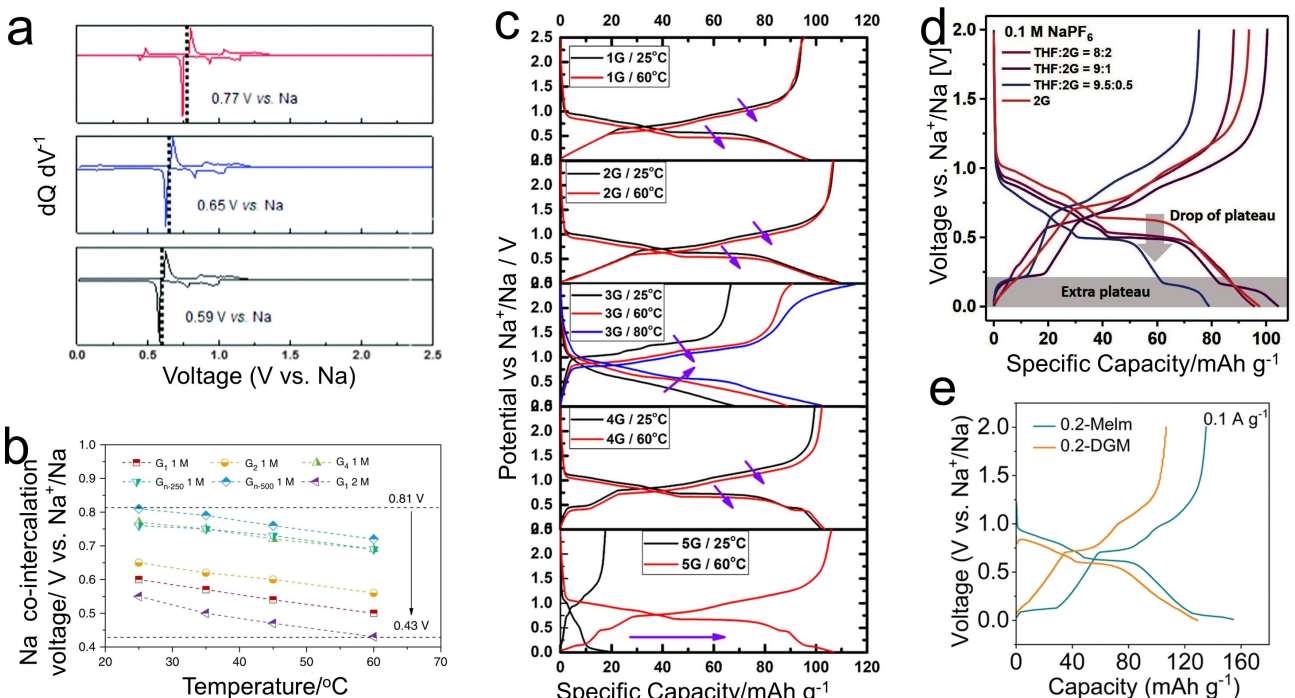


**Figure 5.** (a)  $dQ/dV$  plots showing co-intercalation potential shift with decreasing chain length of ether, tetraglyme (top), diglyme (middle), monoglyme (bottom). Reproduced from ref. [12] with permission from Royal Society of Chemistry. (b) Na co-intercalation voltage with varied solvent, salt content, and testing temperature. Reproduced from ref. [66] with permission from Springer Nature. (c) Voltage profiles of graphite with varied chain length of linear ethers and measurement temperature. Reproduced from ref. [67] with permission from American Chemical Society. (d) Influence of different ratio of THF: diglyme (2 G) on voltage profiles. The electrolyte concentration is fixed to 0.1 M. Reproduced from ref. [77] with permission from John Wiley and Sons. (e) Voltage profiles of graphite in electrolytes with single solvent, diglyme (DGM) and 1-methylimidazolium (Melm). Electrolyte concentration is fixed of 0.2 M. Reproduced from ref. [74] with permission from Royal Society of Chemistry.

ion pairs, resulting in the increase of T and reduction of  $a_{fs}$ . The voltage-temperature coefficient ( $\Delta E/\Delta T$ ) was calculated as  $-2.85 \text{ mV K}^{-1}$  for dilute electrolytes and  $-1.6 \text{ mV K}^{-1}$  for high concentration electrolytes. The short chain length ethers, high concentration electrolytes, and elevated temperature contributed to a remarkable voltage reduction of 0.38 V (Figure 5b).

Apart from redox potential, the intercalation capacity can also be determined by the structure of ether solvents. For example, triglyme- and pentaglyme-based electrolytes cannot activate graphite anodes at room temperature. Such an "inert" behavior can be activated at augmented temperatures, for example, graphite anodes exhibited well-defined voltage plateaus and improved capacities at  $60^\circ\text{C}$  in above electrolytes (Figure 5c).<sup>[67]</sup> The electrochemical performance improvement of graphite in pentaglyme electrolyte is possibly due to the decreased viscosity from 186 mPa at  $20^\circ\text{C}$  to 22.4 mPa at  $80^\circ\text{C}$ . With respect to the triglyme, its voltage profiles differ from other ethers, possibly originated less favorable coordination configuration. Furthermore, intercalation reactions in crown ether-based electrolyte have also been investigated. For example, Goktas et al realized reversible intercalation of  $\text{Na}^+$  in graphite at  $60^\circ\text{C}$  in the 18-crown-ether-6 electrolyte. The capacity is only  $\sim 75 \text{ mAh g}^{-1}$  because of the less flexible ring structure of crown ethers.<sup>[67]</sup>

In an effort to explore the feasibility of other solvents for co-intercalation reaction, Son et al prepared a series of dilute electrolytes using either tetrafurane (THF), or 1,3-dioxolane (DOL) as primary solvents and diglyme as additive (<10 vol%). In these electrolytes, graphite anodes exhibited a capacity of  $90 \text{ mAh g}^{-1}$  with a voltage reduction of 0.2 V for the major redox peaks and a new redox peak at 0.15 V (Figure 5d). It is noted that both THF and DOL were inappropriate for Na ion intercalation reaction in graphite due to their unstable solvation shell.<sup>[44,54,68]</sup> For non-ether-based electrolytes, Maluangnont et al synthesized a series of Na-t-GICs using linear and branched amines-based electrolytes.<sup>[69-71]</sup> A theoretical calculation of these alkylamines-based Na-t-GICs presents negative formation energies, indicating their possibility in cycling SIBs.<sup>[72]</sup> Nonetheless, the amine-based Na-t-GICs showed high chemical reactivity in 0.5 M  $\text{NaPF}_6$  ethylenediamine electrolyte with notable  $\text{H}_2$  evolution during cycling. The addition of diglyme to the  $\text{NaPF}_6$  ethylenediamine electrolyte could suppress the chemical reaction and stabilize the reversible capacities of graphite anodes.<sup>[73]</sup> Figure 5e shows a high reversible capacity of  $128.8 \text{ mAh g}^{-1}$  at  $0.5 \text{ A g}^{-1}$  and low redox potentials of 0.05/0.1 V vs.  $\text{Na}/\text{Na}^+$  for graphite anodes in 0.2 M  $\text{NaCF}_3\text{SO}_3$  1-methylimidazole electrolyte.<sup>[74]</sup> In comparison to diglyme solvent, the 1-methylimidazole with higher donor number and dielectric constant can reinforce the solvation of  $\text{Na}^+$ . The 0.2 M 1-methylimidazole-based electrolyte has lower viscosity and higher ionic conductivity than these of diglyme-based counterpart, thus boosting the reaction kinetics. Notwithstanding these great progresses, enrichment in the type of solvents and efficient approaches to lower the working potentials with enlarged capacities and extended cycle life are still required for graphite anodes.

### 3.4. Significant Volume Changes of Graphite

From the *in-situ* XRD results of graphite anodes in SIBs (Figure 3a), one may note the lattice parameters of graphite can expand by  $\sim 250\%$  after full discharging. Figure 6a displays the typical configuration of intercalated graphite with an interlayer distance of 11.98 Å, which is much larger than the 3.35 Å of pristine graphite.<sup>[12]</sup> Kim et al experimentally measured the volume expansion of a single graphite plate – highly ordered pyrolytic graphite (HOPG) which validated the theoretical prediction of the volume changes.<sup>[12]</sup> To have a comprehensive view about the influence of graphite particle expansion on the electrode stability, Goktas et al. quantified the electrode thickness during discharging and charging using an *in-situ* electrochemical dilatometry (Figure 6b).<sup>[55]</sup> It exhibited an initial increase of the graphite electrode by 95 µm upon sodiation, which almost triples that of the pristine thickness. Such a large expansion presumably would result in considerable exfoliation of graphite flakes and instability of the electrodes. Counter-intuitively, graphite anodes are exceptionally stable with an exceptional cyclic life of over 1000 cycles<sup>[11,35,53]</sup> and minor structural irreversibility.<sup>[35,55]</sup> It was explained that the partial electron of Na is transferred to graphene layers (see the yellow charged gain region in graphene layers in Figure 6a), which forms ionic bonds with electrons donated from in-plane C–C bonds, thus preventing the delamination of graphite.<sup>[12,44]</sup> The interactions between  $\text{Na}^+$  and graphene can be mediated by the polarities of solvents. Rathnayake et al investigated the influence of functionalization of diglyme and binding energy increase in graphene-graphene and  $\text{Na}^+$ -solvent-graphite.<sup>[75]</sup> Jung et al proposed that after the full intercalation of solvated  $\text{Na}^+$  into graphite, there is a 30 meV higher exfoliation energy from the newly introduced van der Waals interaction between diglyme and graphene than that between  $\text{Na}^+$  and graphene. It was also pointed out that there is a hybridization between molecular orbital of alkylamines and  $\sigma$  bonding orbitals of carbon in graphene layer.<sup>[72]</sup> The small solvation shell around  $\text{Na}^+$  possessed a strong electric field to maintain the integrity of graphite and avoid its delamination. Despite the encouraging stability of t-GICs in SIBs, the large volume change is unacceptable for commercial batteries. How to effectively suppress the considerable volume expansion is important.

Adding a specific solvent to diglyme for co-solvent-based electrolyte has been demonstrated effective in decreasing the volume expansion of graphite anodes. Two types of additive solvents, like amines and cyclic ethers, have been explored. Zhang et al reported that the 0.5 M  $\text{NaPF}_6$  ethylenediamine: diglyme (v: v=1:1) electrolyte could suppress the volume expansion to 100%, but the cyclic stability is poor.<sup>[73]</sup> The solvent ratios of above electrolyte were then adjusted to an optimal point of v:v=1:9 for ethylenediamine: diglyme, which can also suppress the initial interlayer expansion of graphite to 100%, in contrast to 175% for diglyme-based electrolyte (Figure 6c).<sup>[76]</sup> This electrolyte has also been demonstrated effective in suppressing the thickness variation (expansion/shrinkage per cycle) in electrode level (17–20% vs. 46–49% in diglyme electrolyte). The decreased volume change may be

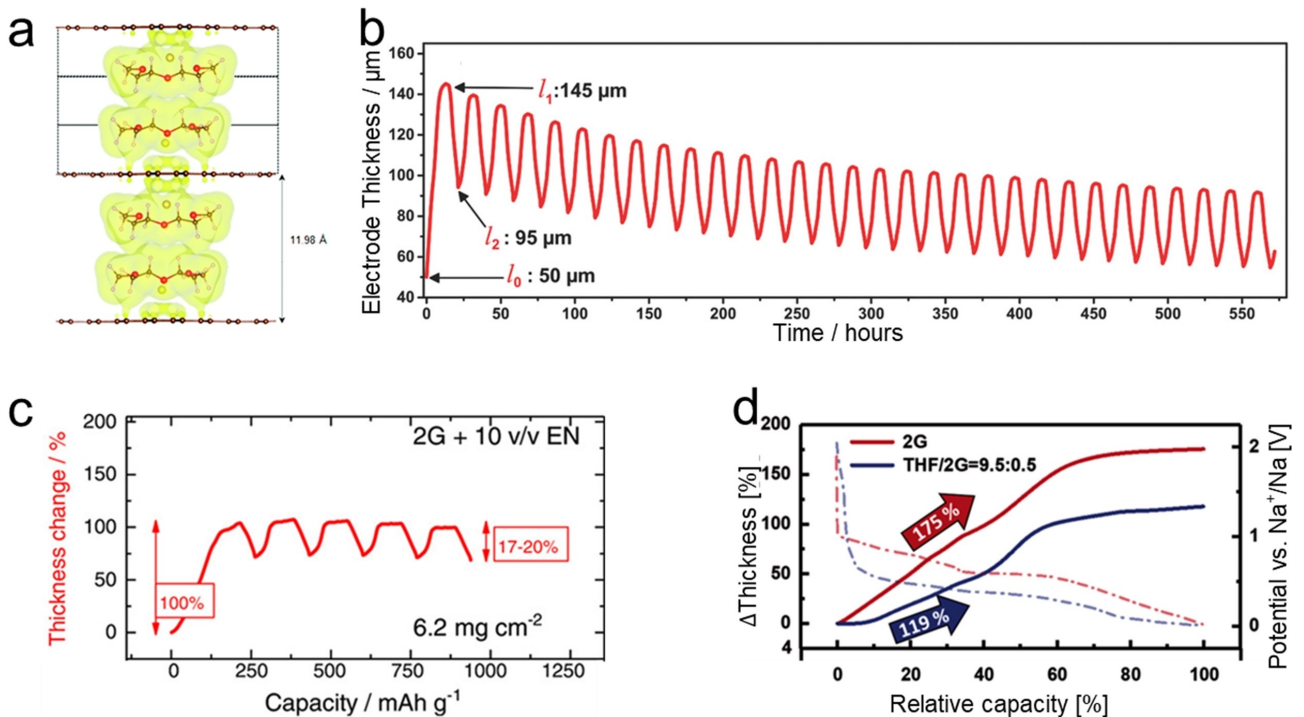


**Figure 6.** (a) Calculated structure with two  $[\text{Na-diglyme}]^+$  complexes situated within galleries of graphite. Reproduced from ref. [12] with permission from Royal Society of Chemistry. (b) Evolution of graphite electrode thickness using diglyme-based electrolyte. Reproduced from ref. [55] with permission from John Wiley and Sons. (c) Evolution of graphite electrode thickness using diglyme-based electrolyte added with 10 vol% ethylenediamine as co-solvent. Reproduced from ref. [76] with permission from John Wiley and Sons. (d) Evolution of graphite electrode thickness using diglyme-based electrolyte and THF-based electrolyte with 5% addition of diglyme. Reproduced from ref. [77] with permission from John Wiley and Sons.

ascribed to the enhanced interaction between graphene layers and intercalated solvents.<sup>[73,76]</sup> The cyclic ethers, like THF, have also been added in diglyme (v: v = 95: 5)-based electrolyte to significantly restrain the volume expansion from 175% (diglyme) to 119% (THF/diglyme) as shown in Figure 6d.<sup>[77]</sup> The utilization of binders with superior mechanical properties is also effective to suppress volume expansions. It was reported that the volume expansion of graphite could be reduced from 175% to 142% when the binder is changed from poly(vinylidene difluoride) (PVDF) to sodium carboxymethyl cellulose (CMC).<sup>[76]</sup> The improvement is probably due to higher Young's modulus of the CMC and enhanced interaction between binder and graphite. Overall, while progresses in mitigating both graphite particle and electrode expansion are promising, it still falls short in meeting the standards of commercial SIBs.

### 3.5. Controversial Insights into SEI

There is a notable capacity loss during the first several cycles of graphite anodes in SIBs, which was attributed to the irreversible electrolyte decomposition and formation of SEI layers on the graphite surface. However, the understandings of SEI on graphite anode in ether-based SIBs are still controversial. Jache et al reported that the pre-formed SEI on the surface of graphite anodes in 0.5 M  $\text{NaSO}_3\text{CF}_3$  in ethylene carbonate/dimethyl carbonate (EC/DMC 1:1 w%) electrolyte blocked the transfer of diglyme- $\text{Na}^+$  complex in the following test in 1 M  $\text{NaPF}_6$  in

diglyme electrolyte, rendering negligible capacities for the first several cycles.<sup>[54]</sup> After continuing the cycling for 25 times, decent capacity ( $\sim 100 \text{ mAh g}^{-1}$ ), high Coulombic efficiency (CE) and well-defined voltage profiles could be recovered. It suggested that the intercalation of solvated  $\text{Na}^+$  may crack the preformed SEI layers in EC/DMC electrolyte. Another preferred hypothesis is that the amount of newly formed SEI is negligible, thus enabling accelerated intercalation of solvated  $\text{Na}^+$ . The negligible SEI can be initially supported by the marginal EIS resistance in Figure 4c.<sup>[35]</sup> The mechanical parameters were also measured for the SEI layers on the surface of t-GIC in SIBs. The pristine graphite flakes exhibited a Young's modulus of 1.99 GPa, which decreased significantly to 435.86 MPa after cycling, implying the formation of a soft SEI layer on the surface of graphite.<sup>[78]</sup> The electrolyte decomposition for SEI formation was further evidenced by an operando tomography and 2D nanomechanical mapping of cycling grid-patterned few-layer graphene using ultrasonic force spectroscopy (Figure 7a).<sup>[79]</sup> During discharging to 0.94 V vs.  $\text{Na}/\text{Na}^+$ , no noticeable change was observed in the tomography images while in the nanomechanical images, the graphene "mesh" changes from blue to light-green. Continued sodiation ends graphene "mesh" by a red contrast. The color evolution is a result of SEI evolution, indicating a stepwise formation of inorganic and organic SEI species. It is proposed that the SEI species generate at different discharging stages.<sup>[78-81]</sup> The chemical compositions of SEI vary with the sodium salts and solvents. For ether-based electrolytes, the typical SEI is thin  $< 10 \text{ nm}$  and comprises rigid inorganics

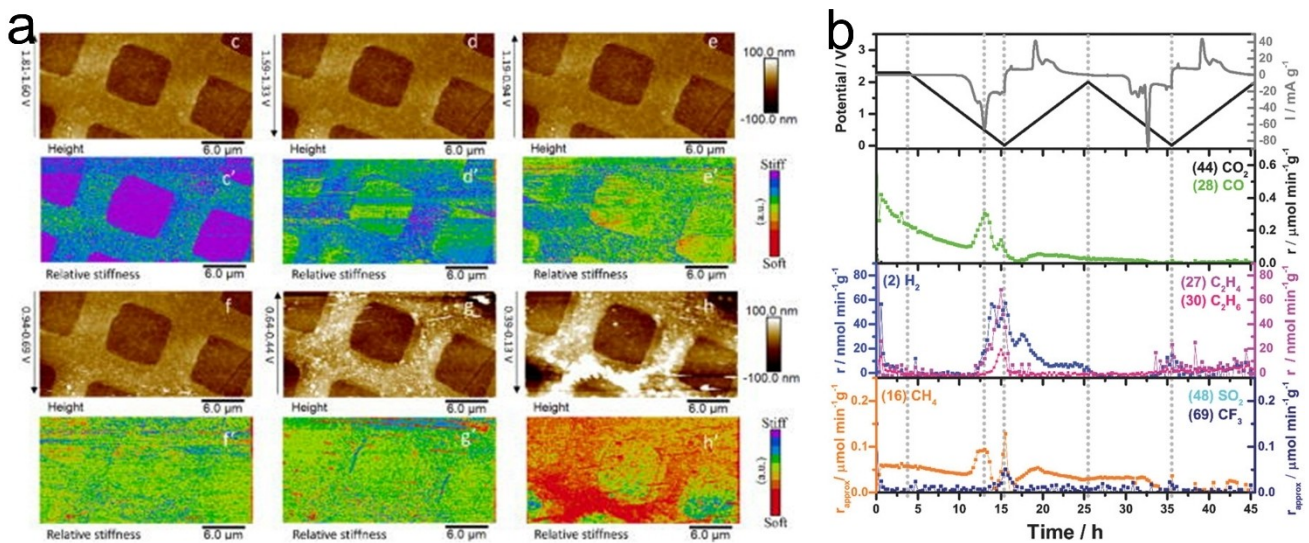


**Figure 7.** (a) Two-dimensional topography images and the corresponding nanomechanical images of electrode surface during the first cathodic scan at different voltage regions measured by ultrasonic force microscopy. Reproduced from ref. [79] with permission from AIP Publishing. (b) Online electrochemical mass spectroscopy results during cycling. Reproduced from ref. [55] with permission from John Wiley and Sons.

(NaF and Na<sub>2</sub>CO<sub>3</sub>) and flexible organics (sodium alkoxides). Wang et al provided insights of aging behavior of SEI at the sodiation states of 60% (corresponding to plateau region) and 100% (referring to the full sodiation).<sup>[80]</sup> After aging, the graphite anode at 60% sodiation showed significant volume contraction (~16 μm decrease in electrode thickness) possibly due to the rearrangement of t-GIC compounds. Such a large structural degradation can break the pre-formed SEI. For the aging of 100% sodiated graphite, the growth of SEI dominates the process, possibly due to the side reactions between electrolyte and Na-t-GIC.

In contrast, Goktas et al provided totally different insights into the SEI chemistry for graphite anodes in SIBs.<sup>[55]</sup> Ex-situ transmission electron microscopy (TEM) results reveal no detectable SEI layers on the surface of graphite. Online electrochemical mass spectrometry (OEMS) results in Figure 7b further ruled out the dynamic evolution of SEI, which only exhibited gas emission from electrolyte decomposition for the first cycle. They suggested that the byproduct of electrolyte decomposition is soluble or volatile rather than being the regular SEI. Zhang et al. corroborated the SEI-free viewpoint by in-situ atomic force microscopy analysis.<sup>[82]</sup> Notable amounts of SEI precipitates appear on graphite surface in 1 M NaClO<sub>4</sub> in EC/PC (1:1 vol%) electrolyte. In contrast, in 1 M NaPF<sub>6</sub> in diglyme electrolyte, no SEI were observed for graphite flakes, instead which exhibited reversible edge-steps and wrinkles during cycling. Overall, further investigation is needed to clarify the existence and the nature of SEI layers on graphite during co-intercalation reactions.

#### 4. Summary and Perspectives

SIBs offer significant advantages over LIBs due to the abundance and low cost of Na resources. The feasibility of

graphite anodes in SIBs has been greatly enhanced by the development of solvated-Na-ion co-intercalation chemistry. Over the past decade, substantial progress has been made in understanding this co-intercalation chemistry. This summary begins by addressing the failure of bare Na<sup>+</sup> intercalation in graphite and then explores the thermodynamic properties and rapid kinetics associated with linear ether solvated-Na<sup>+</sup> intercalation into graphite. The type of solvent plays a crucial role in this chemistry, influencing both the redox potentials of Na ions and the intercalation capacity. Additionally, challenges such as volume expansion and the need for clearer insights into the solvent structure-property relationship are highlighted, with the aim of approaching practical graphite anodes. Building on this foundational research, it is anticipated that co-intercalation chemistry could be extended to multivalent ion battery systems. This extension could provide a theoretical basis for understanding the intercalation mechanisms of multivalent ions in graphite or other layered materials, thereby aiding in the prediction and explanation of some complex behaviors. The experience gained in selecting and optimizing electrolytes and solvents for Na-ion systems has been applied to Ca-ion and Mg-ion battery systems.

Despite these promising developments, several challenges remain in the co-intercalation chemistry of graphite anodes in Figure 8. Possible solutions can be proposed on base of above gained knowledge. First, the capacity limitations can be addressed by optimizing electrolytes, selecting more suitable solvents for Na<sup>+</sup> intercalation, or hybridizing graphite with alloy-type metals owing high capacity. Second, the issue of large volume expansion can be mitigated by inclusion of amine or cyclic ether to linear ether-based electrolytes and use binder owing high Young's modulus and stronger interactions with graphite. Third, the high redox potential associated with solvated-Na-ion intercalation, which reduces the energy density of full cells, can be tackled by developing optimal electrolytes

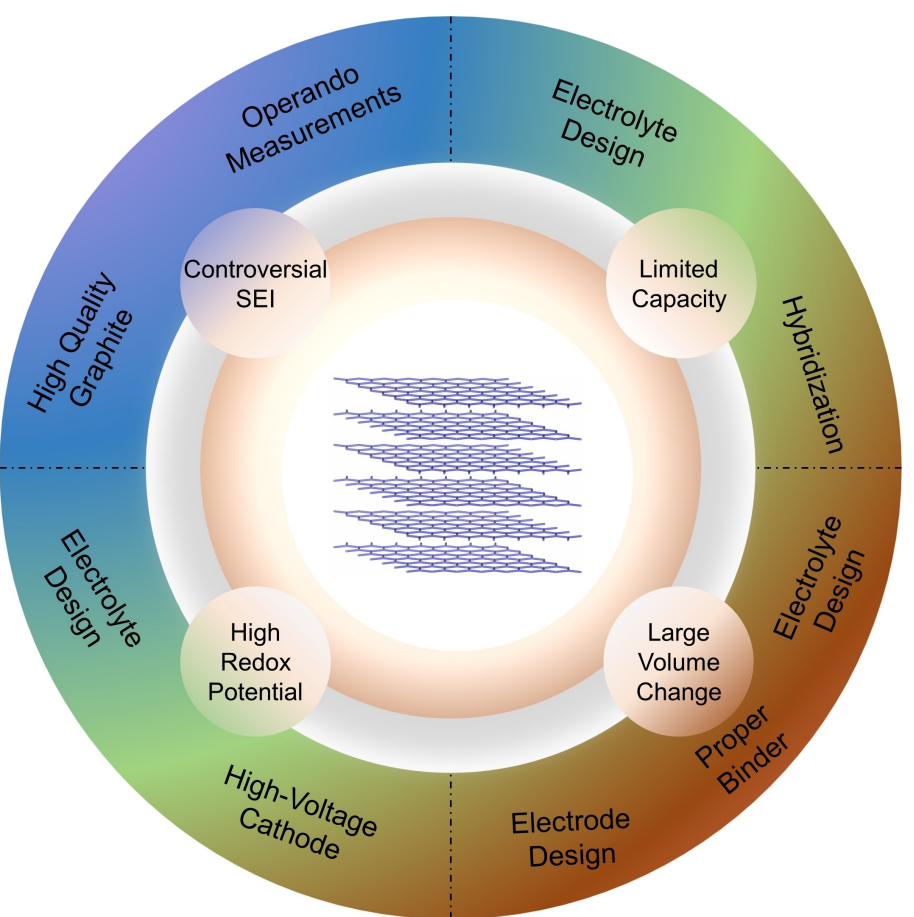


Figure 8. Summary of existing challenges of graphite anode in SIBs and potential resolutions.

by rationally adopting following strategies: (1) using linear ether with short chain length; (2) increasing content of salt; (3) adding co-solvent; (4) replacing ether with imidazole. Besides, find high-voltage cathodes compatible in ether-based electrolytes is also promising. Fourth, more insights to the controversial SEI on graphite are needed. The co-intercalation blocking SEI generated from ester-based electrolytes was confirmed and amendable by transferring to ether-based electrolytes. This observation unambiguously demonstrates the solvent decomposition for SEI formation in carbonate-based electrolytes, which is reasonable from their reduction stabilities. Yet, the nature of SEI on graphite in ether-based electrolytes remains mysterious. Convergence can be realized by more comprehensive characterizations and using defect-less graphite as model materials. Finally, the development of more accurate theoretical models through multi-scale simulation and advanced characterization techniques will deepen our understanding of the co-intercalation mechanism of Na ions. It is believed that ongoing research remains highly valuable to realize the potential of co-intercalation chemistry for graphite electrodes.

## Acknowledgements

The work described in this paper was supported by the Innovation and Technology Fund-Innovation and Technology Support Programme (ITF-ITSP) (Project No. ITS/126/21) from the Innovation and Technology Commission of Hong Kong SAR, Research Centre for Nature-Inspired Science and Engineering (RCNISE) at The Hong Kong Polytechnic University (Project No. 1-CZ23), Environment and Conservation Fund (Project No. ECF/110/2021) from the Environment and Conversion Fund Committee of Hong Kong SAR, and Research Institute for Advanced Manufacturing at the Hong Kong Polytechnic University (Project No. 1-CD4M, 1-45-35-YWCW).

## Conflict of Interests

The authors declare no conflict of interest.

**Keywords:** Co-intercalation · Fast charging · Graphite · Sodium ion battery

[1] H. Wan, J. Xu, C. Wang, *Nat. Chem. Rev.* **2024**, *8*, 30–44.

- [2] M. Chen, X. Ma, B. Chen, R. Arsenault, P. Karlson, N. Simon, Y. Wang, *Joule* **2019**, *3*, 2622–2646.
- [3] Y. Wan, B. Huang, W. Liu, D. Chao, Y. Wang, W. Li, *Adv. Mater.* **2024**, *6*, 2404574.
- [4] J. O. Besenhard, H. P. Fritz, *Angew. Chem. Int. Ed. Engl.* **1983**, *22*, 950–975.
- [5] D. DiVincenzo, E. Mele, *Phys. Rev. B* **1985**, *32*, 2538.
- [6] J. Park, Z.-L. Xu, K. Kang, *Front. Chem.* **2020**, *8*, 432.
- [7] Y. Li, Y. Lu, P. Adelhelm, M.-M. Titirici, Y.-S. Hu, *Chem. Soc. Rev.* **2019**, *48*, 4655–4687.
- [8] D. Stevens, J. Dahn, *J. Electrochem. Soc.* **2001**, *148*, A803.
- [9] P. Ge, M. Fouletier, *Solid State Ionics* **1988**, *28*, 1172–1175.
- [10] K. Nobuhara, H. Nakayama, M. Nose, S. Nakanishi, H. Iba, *J. Power Sources* **2013**, *243*, 585–587.
- [11] B. Jache, P. Adelhelm, *Angew. Chem. Int. Ed.* **2014**, *53*, 10169–10173.
- [12] H. Kim, J. Hong, G. Yoon, H. Kim, K.-Y. Park, M.-S. Park, W.-S. Yoon, K. Kang, *Energy Environ. Sci.* **2015**, *8*, 2963–2969.
- [13] Y. Liu, B. V. Merinov, W. A. Goddard III, *Proc. Nat. Acad. Sci.* **2016**, *113*, 3735–3739.
- [14] D.-M. Kim, S. C. Jung, S. Ha, Y. Kim, Y. Park, J. H. Ryu, Y.-K. Han, K. T. Lee, *Chem. Mater.* **2018**, *30*, 3199–3203.
- [15] S. Takeuchi, K. Miyazaki, F. Sagane, T. Fukutsuka, S.-K. Jeong, T. Abe, *Electrochim. Acta* **2011**, *56*, 10450–10453.
- [16] S. Richard Prabakar, A. B. Ikhe, W. B. Park, K. C. Chung, H. Park, K. J. Kim, D. Ahn, J. S. Kwak, K. S. Sohn, M. Pyo, *Adv. Sci.* **2019**, *6*, 1902129.
- [17] Y. Yi, Y. Xing, H. Wang, Z. Zeng, Z. Sun, R. Li, H. Lin, Y. Ma, X. Pu, M. M. J. Li, *Angew. Chem. Int. Ed.* **2024**, *63*, e202317177.
- [18] J. Park, Z. L. Xu, G. Yoon, S. K. Park, J. Wang, H. Hyun, H. Park, J. Lim, Y. J. Ko, Y. S. Yun, *Adv. Mater.* **2020**, *32*, 1904411.
- [19] F. Chen, Z.-L. Xu, *Microstructures* **2022**, *2*, 2022012.
- [20] M. S. Dresselhaus, G. Dresselhaus, *Adv. Phys.* **1981**, *30*, 139–326.
- [21] A. Ubbelohde, L. Blackman, J. Mathews, *Nature* **1959**, *183*, 454–456.
- [22] A. Ubbelohde, *Carbon* **1972**, *10*, 201–206.
- [23] M. Armand, P. Touzain, *Mater. Sci. Eng.* **1977**, *31*, 319–329.
- [24] J. Seel, J. Dahn, *J. Electrochem. Soc.* **2000**, *147*, 892.
- [25] J. Besenhard, *Carbon* **1976**, *14*, 111–115.
- [26] J. Amiel, P. Delhaes, F. Beguin, R. Setton, *Mater. Sci. Eng.* **1977**, *31*, 243–247.
- [27] D. Billaud, A. Pron, F. L. Vogel, *Synth. Met.* **1980**, *2*, 177–184.
- [28] A. Chenite, D. Billaud, *Carbon* **1982**, *20*, 120–121.
- [29] U. Hofmann, A. Frenzel, Z. *Elektrochem. Angew. Phys. Chem.* **1931**, *37*, 613–618.
- [30] A. Schleede, M. Wellmann, *Z. Phys. Chem.* **1932**, *18*, 1–28.
- [31] W. Tiedemann, *J. Electrochem. Soc.* **1974**, *121*, 1308.
- [32] M. Ichikawa, T. Kondo, K. Kawase, M. Sudo, T. Onishi, K. Tamaru, *J. Chem. Soc. Chem. Commun.* **1972**, 176–177.
- [33] R. Fong, U. Von Sacken, J. R. Dahn, *J. Electrochem. Soc.* **1990**, *137*, 2009.
- [34] M. R. Wagner, J. Albering, K.-C. Moeller, J. Besenhard, M. Winter, *Electrochem. Commun.* **2005**, *7*, 947–952.
- [35] H. Kim, J. Hong, Y. U. Park, J. Kim, I. Hwang, K. Kang, *Adv. Funct. Mater.* **2015**, *25*, 534–541.
- [36] M.-Y. Sun, F.-D. Yu, Y. Xia, L. Deng, Y.-S. Jiang, L.-F. Que, L. Zhao, Z.-B. Wang, *Chem. Eng. J.* **2022**, *430*, 132750.
- [37] G. Alvarez Ferrero, G. Ávall, K. A. Mazzio, Y. Son, K. Janßen, S. Risso, P. Adelhelm, *Adv. Energy Mater.* **2022**, *12*, 2202377.
- [38] J. Park, S. J. Kim, K. Lim, J. Cho, K. Kang, *ACS Energy Lett.* **2022**, *7*, 3718–3726.
- [39] T. Huang, Z. Liu, F. Yu, F. Wang, D. Li, L. Fu, Y. Chen, H. Wang, Q. Xie, S. Yao, *ACS Appl. Mater. Interfaces* **2020**, *12*, 52635–52642.
- [40] C. Zhang, P. Chandan Solanki, D. Cao, H. Zhao, Y. Lei, *ACS Appl. Mater. Interfaces* **2023**, *15*, 24459–24469.
- [41] M. L. Divya, Y.-S. Lee, V. Aravindan, *J. Power Sources* **2022**, *543*, 231823.
- [42] K. Subramanyan, V. Aravindan, *ACS Energy Lett.* **2022**, *8*, 436–446.
- [43] M. L. Divya, Y.-S. Lee, V. Aravindan, *ACS Energy Lett.* **2021**, *6*, 4228–4244.
- [44] G. Yoon, H. Kim, I. Park, K. Kang, *Adv. Energy Mater.* **2017**, *7*, 1601519.
- [45] S. C. Jung, Y.-J. Kang, Y.-K. Han, *Nano Energy* **2017**, *34*, 456–462.
- [46] D. Stevens, J. Dahn, *J. Electrochem. Soc.* **2000**, *147*, 1271.
- [47] Y. Cao, L. Xiao, M. L. Sushko, W. Wang, B. Schwenzer, J. Xiao, Z. Nie, L. V. Saraf, Z. Yang, J. Liu, *Nano Lett.* **2012**, *12*, 3783–3787.
- [48] Y. Wen, K. He, Y. Zhu, F. Han, Y. Xu, I. Matsuda, Y. Ishii, J. Cumings, C. Wang, *Nat. Commun.* **2014**, *5*, 4033.
- [49] Y. Okamoto, *J. Phys. Chem. C* **2014**, *118*, 16–19.
- [50] Y. Kondo, T. Fukutsuka, K. Miyazaki, Y. Miyahara, T. Abe, *J. Electrochem. Soc.* **2019**, *166*, A5323.
- [51] Z. Wang, S. M. Selbach, T. Grande, *RSC Adv.* **2014**, *4*, 4069–4079.
- [52] J. Zhao, X. Zou, Y. Zhu, Y. Xu, C. Wang, *Adv. Funct. Mater.* **2016**, *26*, 8103–8110.
- [53] A. P. Cohn, K. Share, R. Carter, L. Oakes, C. L. Pint, *Nano Lett.* **2016**, *16*, 543–548.
- [54] B. Jache, J. O. Binder, T. Abe, P. Adelhelm, *Phys. Chem. Chem. Phys.* **2016**, *18*, 14299–14316.
- [55] M. Goktas, C. Bolli, E. J. Berg, P. Novák, K. Pollok, F. Langenhorst, M. v. Roeder, O. Lenchuk, D. Mollenhauer, P. Adelhelm, *Adv. Energy Mater.* **2018**, *8*, 1702724.
- [56] K. Gotoh, H. Maruyama, T. Miyatou, M. Mizuno, K. Urita, H. Ishida, *J. Phys. Chem. C* **2016**, *120*, 28152–28156.
- [57] W. A. Henderson, *J. Phys. Chem. B* **2006**, *110*, 13177–13183.
- [58] H. Bock, C. Näther, Z. Havlas, A. John, C. Arad, *Angew. Chem. Int. Ed. Engl.* **1994**, *33*, 875–878.
- [59] G. Ávall, G. A. Ferrero, K. A. Janßen, M. Exner, Y. Son, P. Adelhelm, *Adv. Energy Mater.* **2023**, *13*, 2301944.
- [60] S. Thinius, M. M. Islam, P. Heitjans, T. Bredow, *J. Phys. Chem. C* **2014**, *118*, 2273–2280.
- [61] Z. Xu, X. Lv, J. Chen, L. Jiang, Y. Lai, J. Li, *Carbon* **2016**, *107*, 885–894.
- [62] C.-J. Yu, S.-B. Ri, S.-H. Choe, G.-C. Ri, Y.-H. Kye, S.-C. Kim, *Electrochim. Acta* **2017**, *253*, 589–598.
- [63] C. Sun, X. Ji, S. Weng, R. Li, X. Huang, C. Zhu, X. Xiao, T. Deng, L. Fan, L. Chen, *Adv. Mater.* **2022**, *34*, 2206020.
- [64] S. Lei, Z. Zeng, M. Liu, H. Zhang, S. Cheng, J. Xie, *Nano Energy* **2022**, *98*, 107265.
- [65] L. Seidl, N. Bucher, E. Chu, S. Hartung, S. Martens, O. Schneider, U. Stimming, *Energy Environ. Sci.* **2017**, *10*, 1631–1642.
- [66] Z.-L. Xu, G. Yoon, K.-Y. Park, H. Park, O. Tamwattana, S. Joo Kim, W. M. Seong, K. Kang, *Nat. Commun.* **2019**, *10*, 2598.
- [67] M. Goktas, B. Akduman, P. Huang, A. Balducci, P. Adelhelm, *J. Phys. Chem. C* **2018**, *122*, 26816–26824.
- [68] Q. Liu, F. Wu, D. Mu, B. Wu, *Phys. Chem. Chem. Phys.* **2020**, *22*, 2164–2175.
- [69] T. Maluangnont, G. T. Bui, B. A. Huntington, M. M. Lerner, *Chem. Mater.* **2011**, *23*, 1091–1095.
- [70] T. Maluangnont, K. Gotoh, K. Fujiwara, M. M. Lerner, *Carbon* **2011**, *49*, 1040–1042.
- [71] T. Maluangnont, W. Sirisaksoontorn, M. M. Lerner, *Carbon* **2012**, *50*, 597–602.
- [72] G.-C. Ri, C.-J. Yu, J.-S. Kim, S.-N. Hong, U.-G. Jong, M.-H. Ri, *J. Power Sources* **2016**, *324*, 758–765.
- [73] H. Zhang, Z. Li, W. Xu, Y. Chen, X. Ji, M. M. Lerner, *Nanotechnology* **2018**, *29*, 325402.
- [74] W. Zhao, C. Wang, Z. Cheng, C. Zheng, Q. Yao, J. Pan, X. Ma, J. Yang, *Chem. Sci.* **2024**, *15*, 6500–6506.
- [75] R. Rathnayake, D. J. Searles, T. T. Duignan, X. Zhao, *Phys. Chem. Chem. Phys.* **2023**, *25*, 19106–19115.
- [76] I. Escher, Y. Kravets, G. A. Ferrero, M. Goktas, P. Adelhelm, *Energy Technol.* **2021**, *9*, 2000880.
- [77] Y. Son, G. Ávall, G. A. Ferrero, A. I. Freytag, I. Escher, K. A. Janßen, M. Jauregui, D. Saurel, M. Galceran, P. Adelhelm, *Batteries & Supercaps* **2024**, *7*, e202300506.
- [78] Z. Wang, H. Yang, Y. Liu, Y. Bai, G. Chen, Y. Li, X. Wang, H. Xu, C. Wu, J. Lu, *Small* **2020**, *16*, 2003268.
- [79] Y. Chen, S. Zhang, W. Zhang, A. Quadrelli, S. Jarvis, J. Chen, H. Lu, N. Mangayarkarasi, Y. Niu, J. Tao, *Appl. Phys. Rev.* **2024**, *11*, 021422.
- [80] J. Wang, J. Hu, F. Kang, D. Zhai, *Energy Environ. Sci.* **2024**, *17*, 3202–3209.
- [81] J. Maibach, F. Jeschull, D. Brandell, K. Edstrom, M. Valvo, *ACS Appl. Mater. Interfaces* **2017**, *9*, 12373–12381.
- [82] X.-R. Zhang, J.-Y. Yang, Z.-Y. Ren, K.-Y. Xie, Q. Ye, F. Xu, X.-R. Liu, *New Carbon. Mater.* **2022**, *37*, 371–379.
- [83] K. Kubota, M. Dahbi, T. Hosaka, S. Kumakura, S. Komaba, *Chem. Rec.* **2018**, *18*, 459–479.

Manuscript received: July 31, 2024

Revised manuscript received: September 2, 2024

Accepted manuscript online: September 4, 2024

Version of record online: October 23, 2024